Journal of Magnetism and Magnetic Materials 499 (2020) 166297

Contents lists available at ScienceDirect

Journal of Magnetism and Magnetic Materials

journal homepage: www.elsevier.com/locate/jmmm

Electronic structure and spin polarization of Co/black phosphorus interface

Baoxing Liu[a], Haipeng Xie[a,*], Yuquan Liu[a], Can Wang[a], Shitan Wang[a], Yuan Zhao[a], Jinxin Liu[a], Dongmei Niu[a], Han Huang[a], Yongli Gao[a,b,*]

[a] Hunan Key Laboratory of Super-microstructure and Ultrafast Process, School of Physics and Electronics, Central South University, Changsha, Hunan 410083, PR China
[b] Department of Physics and Astronomy, University of Rochester, Rochester, NY 14627, USA

ARTICLE INFO

Keywords:
Co
Black phosphorus
Spin-resolved photoemission spectroscopy
Interfacial electronic structure

ABSTRACT

We studied the electronic properties and spin polarization of the interface between Co and black phosphorus (BP) with ultraviolet, X-ray and spin-resolved photoemission spectroscopy. The results show that the outermost BP is destroyed and the unbonded P is produced in the process of Co deposition. There is no chemical reaction and an interface dipole is found at the Co/BP interface. The SR-UPS results show that there is an inverted spin polarization near E_F and the spin polarization is about positive 10%, which is attributed to the interface hybridization between Co and BP.

1. Introduction

2D materials have been developed rapidly owing to their interesting properties and wide potential applications. Graphene, a typical 2D material, possesses many useful electrical and mechanical properties [1–5], but the zero-band gap hinders its applications [6,7]. In order to solve this problem, other 2D materials with finite band gaps such as transition metal dichalcogenides (TMDCs) have been investigated [8,9]. However, due to the higher spin-orbit coupling, spin transport in TMDs is largely eclipsed. Thus, it is necessary to find new 2D materials with bandgap and low spin-orbit coupling for spintronic devices [10]. Black phosphorus (BP) is a 2D material with a layered structure, which has unique electrical and optical properties, and plenty of BP-based devices have been fabricated [11–15]. In contrast to the TMDs, relatively lighter P atoms leads to low spin-orbit coupling, making BP more favorable for spin transport [16]. Unlike graphene, there exists an intrinsic direct band gap in BP [17–20], and its value can be modified by changing the thickness, strain and electric fields [21,22]. The BP-based spin valve has been studied both theoretically and experimentally [7,23,24]. Thus, BP has an enormous potential in the application of innovative spintronic devices.

Co is among the most commonly used ferromagnetic electrode for both injection and detection of spin-polarized current [25,26]. Sui et al. present a density functional theory study of Co atoms adsorbed on a phosphorene sheet and found that the Co atom can bond strongly to the phosphorene with sizable binding energies [27]. The Co/phosphorene systems exhibit interesting magnetic properties, which arise from the exchange splitting of the Co 3d orbitals. Kamalakar et al. investigated the field-effect transistor characteristics of nanolayers of BP with TiO_2/Co contacts [10]. The results show that ambipolar transistor with $I_{on}/I_{off} > 10^4$ and on-state current reaching 150 $\mu A \cdot \mu m^{-1}$ in the hole conduction regime. The spin injection is mainly from the Fermi surface, so the spin polarization of Fermi surface is of great significance. Schulz et al. found that the presence of the LiF layer reverses the spin polarization in the Alq_3. This is due to a change of extracted spin polarization brought about by a vacuum level shift due to the electric dipole moment induced by the LiF [28]. Sun et al. reported that a thin ferroelectric interfacial layer was added between the ferromagnetic electrode and the organic spacer to regulate the resistance of organic spin valves. The magnetoresistance changes sign when the electric polarization of the ferroelectric layer is reversed [29]. Barraud et al. fabricated a nanoscale Co-based magnetic tunnel junction with a magnetoresistance response of up to 300% and developed a spin transport model that describes the role of interfacial spin-dependent metal/molecule hybridization on the effective polarization allowing enhancement and sign reversal of injected spins, which bring new electrical functionalities to spintronics devices [30]. Atodiresei et al. reported that the hybridization of the out-of-plane p_z atomic-type orbitals with the d states of the metal led to the inversion of the spin polarization at the organic site [31]. Despite the interesting observations, the electronic structures of ferromagnetic/semiconductor interfaces are still not clear. Given the interesting properties of BP, it is necessary to investigate the electronic structure to understand and explore the spintronic device potential of this promising material.

* Corresponding authors at:Hunan Key Laboratory of Super-microstructure and Ultrafast Process, School of Physics and Electronics, Central South University, Changsha, Hunan 410083, PR China.
E-mail addresses: xiehaipeng@csu.edu.cn (H. Xie), ygao@pas.rochester.edu (Y. Gao).

https://doi.org/10.1016/j.jmmm.2019.166297
Received 4 September 2019; Received in revised form 28 November 2019; Accepted 12 December 2019
Available online 14 December 2019

In this article, we study the electronic structure at the Co/BP interface using ultraviolet, X-ray and spin-resolved ultraviolet photoemission spectroscopy (UPS, XPS and SR-UPS). Our observations show that there are strong interactions at the interface and the outermost BP is destroyed at the initial deposition of Co. An interface dipole is observed at the Co/BP interface and the spin polarization of 3 nm Co deposition on BP is about positive 10%. The results provide some understanding for the development of spintronic devices based on Co/BP.

2. Experimental method

The experiment was carried out in an interconnected ultrahigh vacuum system. First, in the preparation chamber, the BP single crystal purchased from HQ Graphene was mechanically peeled off with a scotch tape. The base pressure of the preparation chambers is better than 1.5×10^{-8} mbar, and the rest of the chamber base pressure is better than 2×10^{-10} mbar. In the analysis chamber, the sample quality was tested by XPS and low energy electron diffraction (LEED). To perform a UPS measurement, a bias of -5 V was applied to the sample in order to observe the secondary electron cutoff. The analysis chamber is equipped with a SPECS PHPIBOS 150 hemispherical energy analyzer, a Microwave UV Light Source (He I, $h\nu = 21.2$ eV), and a monochromatic Microfocus X-ray Source (Al K_α, $h\nu = 1486.7$ eV). In the molecular beam epitaxy chamber (MBE), Co layers were deposited on BP and the thickness monitored with quartz crystal microbalance. After the sample was magnetized, its spin polarization was measured with a Mott detector. The effective Sherman factor S_{eff} of the Mott detector is 0.12. For more information about the experimental equipment can refer to Refs. [32–36]. The prepared samples were taken out of the vacuum system and subjected to X-ray Diffraction (XRD) and Raman scattering spectra tests. The structure was characterized with XRD using a Bruker SIMENS D500 and the 2θ step-scanning was carried out from 10° to 70° with a step size of 0.02°. The Raman measurements were performed under the excitation of a 514 nm laser in a Renishaw inVia Qontor system. The sample transport process was under the protection of nitrogen. The experiment was carried out at room temperature.

3. Results and discussion

Fig. 1(a) shows the layered crystal structure of bulk black phosphorus and stacked together by van der Waals force, indicating that a clean BP surface can be obtained by mechanical exfoliation in ultrahigh vacuum. The XPS full scan spectra of mechanical exfoliation of BP are shown in Fig. 1(b), and there is no other peak except P 2p peak located at ca. 130.32 eV. Fig. 1(c) shows a clear LEED pattern and it exhibits integrity crystal structure without reconstructions. According to Fig. 1(b) and (c), a high-quality BP surface was obtained by mechanical peeling in ultrahigh vacuum.

Fig. 2 shows the UPS spectra evolve with the thickness of Co deposited on BP. For clarity, all spectra were normalized to the same height. Shown in Fig. 2(a) are the cut-off region which determined by linear extrapolation. The WF of intrinsic BP is 4.24 eV, in agreement with the previous reports [37]. At 1 Å Co thickness, the WF is 4.37 eV, increases with the subsequent deposition of Co, approaching to the maximum 4.66 eV after the deposition of 4 Å Co, the total shift is 0.42 eV. With further increasing of the Co thickness, the WF decreases to 4.53 eV at 15 Å, then increases slowly and saturates at 5.03 eV at 90 Å. Fig. 2(b) are the valence band (VB) region. The valence band maximum (VBM) of intrinsic BP is 0.1 eV. It shifts toward the E_F with the Co deposition and the metallic Fermi level cutoff starts to appear as Co thickness reaches 4 Å. To track the change of VBM, we used the dotted lines mark the VB peak of BP. The peak value located near 2.36 eV and it shifts 0.25 eV after 1 Å Co deposition. The possible reason is that the interface hybridization between Co and BP leads to the change of interface electronic structure [38,39]. Fig. 2(c) display the energy level alignment diagram at Co/BP interface. It is found that the WF increases first, decreases from 4 Å to 30 Å, and then increases again with the further increasing of Co thickness. At the Co/BP interface, there is an interface dipole of 0.13 eV pointing from the BP to the Co side, arising from the charge redistribution.

We investigated the samples chemical characteristics by using XPS. All spectra were normalized to the same height for visual clarity and the BE of the peak center was obtained by fitting Gaussian-Lorentzian peaks. Fig. 3 shows Co $2p_{3/2}$ and P 2p core level evolves with thickness of Co deposited on BP. At the initial Co deposition, the Co $2p_{3/2}$ peak is located at 779.17 eV for 1 Å Co thickness, as shown in Fig. 3(a). With the subsequent deposition, the Co $2p_{3/2}$ peak shifts toward lower BE and reaches the minimum BE of 778.42 eV at 90 Å, the total shift is 0.75 eV. The possible reason is that the interface hybridization between Co and BP at lower Co coverage [40,41]. Otherwise, there is no chemical reaction between Co and BP because of the Co $2p_{3/2}$ shows only one peak as the increasing of Co thickness. Fig. 3(b) shows the core level of P 2p is a doublet consisting of P $2p_{3/2}$ and P $2p_{1/2}$. Translucent red peak corresponds to the P $2p_{3/2}$ peak of lattice P component, it located at ca. 130.27 eV. With the increasing Co thickness, a new translucent red peak appeared at 129.92 eV, corresponding to the unbonded P atoms [37,42]. Metal materials deposited on the BP usually cause chemical disorder at the interface, the bombardment of 'high-energy' metal atoms and heating of the contact region will damage the crystal lattice [43–45]. The initial deposition of Co destroys the outermost BP structure and produce unbonded P atoms. As the thickness of the Co deposition increase, the unbonded P component increases, after 4 Å, its component proportion larger than the lattice P, and after 30 Å, there is no lattice P component.

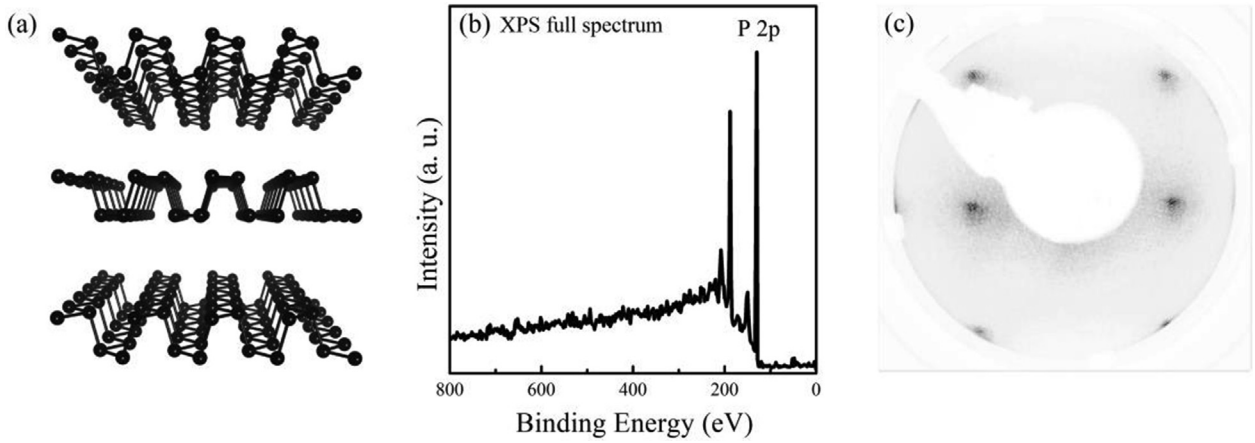

Fig. 1. (a) The crystal structure of layered bulk BP. (b) XPS full spectra of BP. (c) LEED patterns of bulk BP.

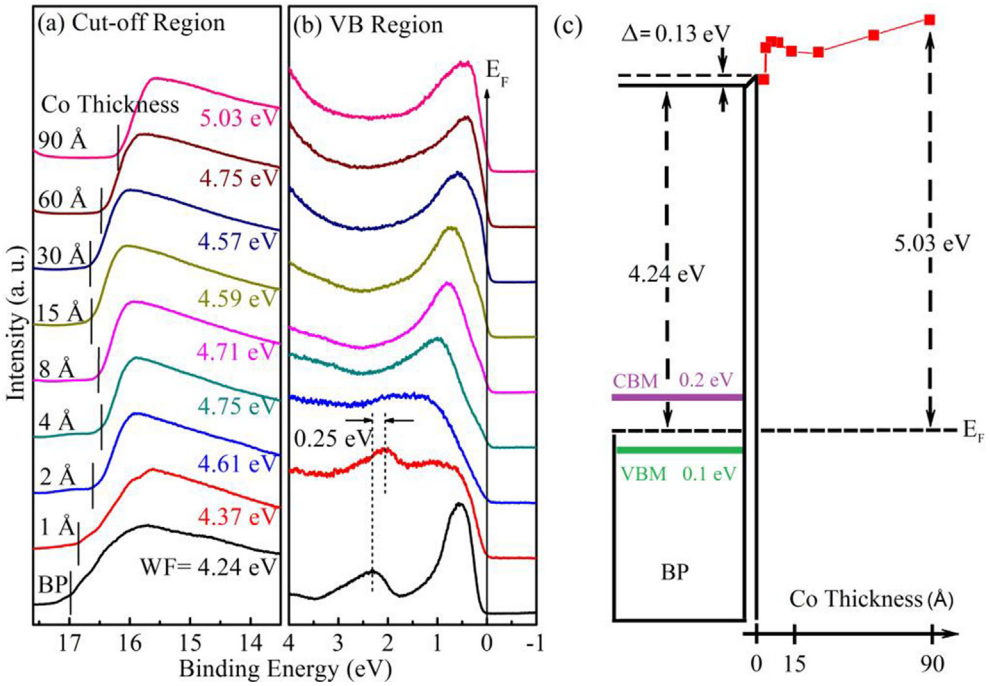

Fig. 2. UPS spectra evolves with thickness of Co deposited on BP. (a) The cut-off region. (b) The VB edge region. (c) The energy level diagram of the Co/BP interface.

To further analyze the process of the growth of Co on BP film, we focus on the XPS intensity attenuation by the Co overlayer. The intensity attenuation of photoelectrons after passing through an Co overlayer (I_{Co}) [46]

$$I_{Co} = I_{90}\cdot[1 - \exp(-d/\lambda_{Co})] \quad (1)$$

or that from the BP substrate (I_{BP})

$$I_{BP} = I_0\cdot\exp(-d/\lambda_{BP}) \quad (2)$$

where I_{90} is the photoelectron intensities from the 90 Å Co overlayer and I_0 is the photoelectron intensities from the BP substrate without the Co overlayer, d is the Co overlayer thickness, and λ_{Co} (λ_{BP}) is the mean free path (MFP) of photoexcited electrons in Co (P). The intensity is based on the peak area of the elements which was obtained by fitting Gaussian-Lorentzian peaks, followed by normalization with corresponding relative atomic sensitivity factors. The attenuation, based on Eq. (1) and (2), of the XPS peaks of the Co overlayer or BP substrate can be used to figure out the growth mode of Co deposition onto BP substrate [47,48].

As shown in Fig. 3c, for the photoelectrons ejected from the Co 2p of

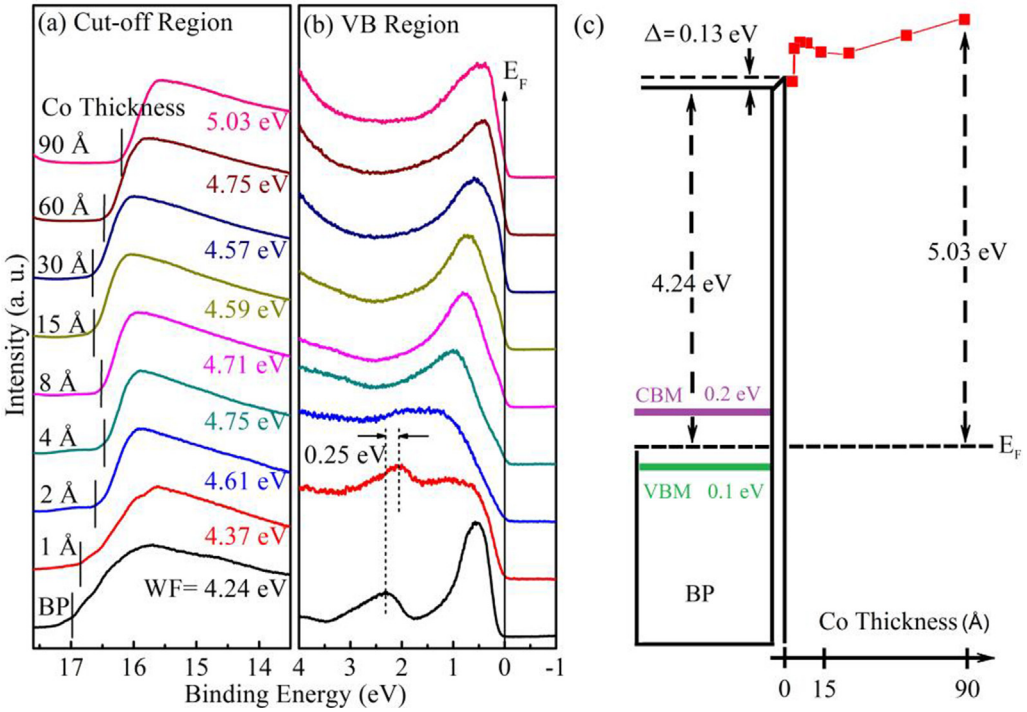

Fig. 3. XPS spectra evolves with thickness of Co deposited on BP. (a) Co $2p_{3/2}$, (b) P 2p, (c) The photoelectron intensity as a function of the thickness of Co coverage.

the Co/BP film, the intensities attenuate gradually with increasing thickness of Co coverage up to 15 Å, and decrease sharply with thicker Co coverage. At the lower Co coverages, *i.e.* $\Theta < 15$ Å, the photoelectron intensity decreases gently at first, which confirmed by a small slope for the Co 2p as shown with a dash dotted line in the figure. The slope curve is obtained by linearly fitting the experimental data of $\Theta < 15$ Å. With enough thickness of the Co coverage, *i.e.* $\Theta > 15$ Å, a sharper decrease of photoelectron intensity is achieved by subsequent deposition of Co. For the photoelectrons ejected from the BP, the intensities attenuate sharply with increasing thickness of Co coverage up to 4 Å, and decrease gradually with increasing thickness up to 30 Å, which can be confirmed by a relatively large slope for the BP as shown with a dash line in the figure. Formation of Co clusters can be excluded at lower Co coverages from the attenuation of the P signals. The data lead to an electron escape depth of ~10 Å, not agreeing with the expected value [49]. It can be attributed to the outermost BP flake lattice being destroyed by the deposition of Co. At the initial deposition of Co, the outermost BP lattice is destroyed and turn to unbonded P. The intensities attenuate gradually can be attributed to some unbonded P atoms segregate at the surface. With the subsequent deposition, the photoelectrons intensities of P 2p attenuate sharply, because of the photoelectrons are suppressed by the Co coverage, indicating that the amount of unbonded P is the most at 4–30 Å. Combined with XPS and UPS spectra, it can be inferred that the interface hybridization between Co and BP is a predominant role in the initial Co deposition, *i.e.* $\Theta < 4$ Å, which lead to the increasing of WF. With the increasing of Co thickness, the destruction of outermost BP crystal lattice is the main reason caused the change of WF, the surface segregated unbonded P atoms will reduce the WF. With enough thickness of the Co coverage, *i.e.* $\Theta > 30$ Å, no more unbonded P atoms segregated at the surface, the WF increases again.

These observations reveal that interfacial disruption between the metal layer and BP film is a fundamental problem that may hurt the device performance. As shown in Fig. 3(a), we can find that the Co core level shift to low binding energy at low coverage (*i.e.* $\Theta < 8$ Å). It is different with our pervious report in Au/BP, which keep unchanged until 4 Å Au [37]. Similarly, the VB of BP also keep unchanged in Au/BP interface, but that shift to Fermi level in Co/BP interface as shown in Fig. 2(b), indicating that the interface hybridization does occur between Co and BP at lower Co coverage.

In order to further investigate the change of the crystalline structure of Co/BP interface, we compared the XRD patterns and Raman scattering spectra before (black line) and after (red line) 30 Å Co deposition. As shown in Fig. 4(a), it is find that the position of all the diffraction peaks keep unchanged and the intensity obviously attenuate after 30 Å Co deposition. Meanwhile, there is no diffraction peak of Co in the XRD patterns, indicating that the Co film did not crystallize. As shown in Fig. S2, the BP LEED pattern disappeared, and no new LEED pattern emerged after 30 Å Co deposition. This also confirmed that the Co film is amorphous. Attenuation trend of intensity is also observed in Raman scattering spectra, as shown in Fig. 4(b). The vibration mode A_g^1 is corresponding to the out-of-plane vibration mode and its wave number is 361.9 cm^{-1}. The vibration mode B_{2g} and A_g^2 are corresponding to the in-plane vibration mode and their wave numbers are 437.64 and 465.74 cm^{-1} respectively, in agreement with the pervious report [50]. In the above analysis, we find that the BP has been destroyed and turn to unbonded P. In order to verify if the BP or unbonded P unites with Co and forms Co_2P or CoP. We have compared the XRD patterns and Raman scattering spectra of BP, 30 Å Co/BP and Co_2P or CoP [51,52]. It is found that the characteristic peaks are different, indicated that the BP or unbonded P does not react with Co and form Co_2P or CoP during the deposition of Co film. Combine with the XPS results, it can be speculated that the destruction of BP take place in Co/BP interface but there is no chemical reaction.

It is well known that the spin polarization of Co thin film is crucial for Co-based spintronic devices, so it is especially important to see

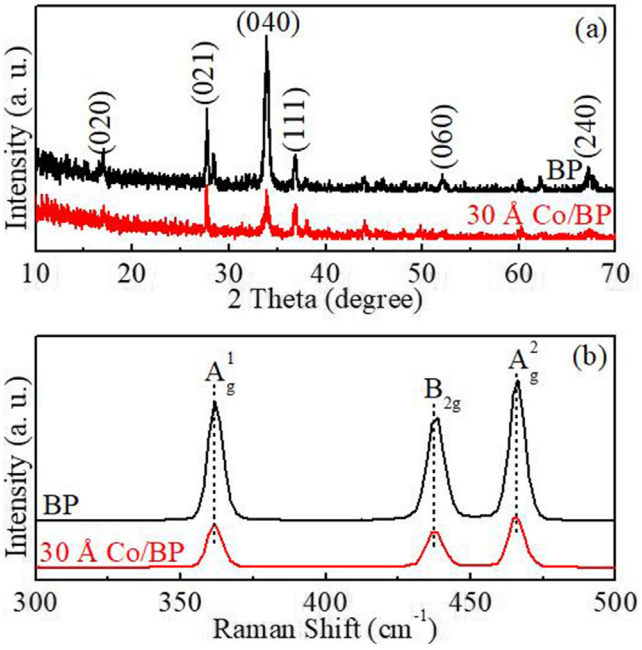

Fig. 4. (a) XRD patterns and (b) Raman scattering spectra of the BP and 30 Å Co/BP.

whether any spin polarization of Co thin film at the Co/BP interface. Fig. 5(a) and (c) show the spin-polarized ultraviolet photoemission spectra of bulk BP. Black lines (spin-up) and red lines (spin down) represents fitting results with the polynomial function. The original curve is shown in translucent color. We can find that there is no spin polarization of bulk BP. Fig. 5(b) and (d) show the spin-polarized photoemission spectra of 3 nm Co deposited on BP films and the spin polarization of Co is approximately positive 10%. Generally, the spin polarization of Co thin film is negative close to Fermi level [53], see the Supporting Information Fig. S1, but the spin polarization of the 3 nm Co/BP film inverted near the Fermi surface as shown in Fig. 5(d). The inverted spin polarization near EF can be attributed to the interface hybridization between Co and BP electronic orbitals. Due to the existence of the lone pair electrons on P atoms in phosphorene, Co orbitals can hybridize with those of phosphorene. Sui et al. reported that the increasing d electrons would fill the spin-down states when the Co atoms adsorbed at the surface of phosphorene [27]. The spin-up and spin-down channels of Co 3d orbitals are fully and partially occupied, respectively, making it have magnetic moment. For an isolated Co atom, the 4 s orbitals are lower in energy than the 3d orbitals. When the Co atoms adsorbed at the surface of phosphorene, the large Coulomb repulsion between the phosphorene and the Co 4 s orbitals will push up the 4 s orbitals, therefore causing the charge transfer from the 4 s orbitals to the 3d orbitals. The increasing d electrons further fill the spin-down states in sequence, and therefore, induce a decrease in the net magnetic moments. Thus, the molecular structure of BP has been destroyed, but spin polarization of Co film can be detected after the growth of 3 nm cobalt, and the inverted spin polarization can be attributed to the interface hybridization between Co and BP. The BP structure should not be damaged as much as possible for the application potential of Co/BP-based spintronic devices. The preferable approach is to insert a modification layer at the interface to avoid damage [28,54]. The second way is called buffer layer assisted growth which is to condense inert gas on the surface to form a buffer layer at low temperature before Co deposited [55]. The third way is called indirect deposition which is intentionally filled with inert gas in the vacuum chamber during Co deposited and the Co sources and sample surface toward the same direction [56]. Understanding the interface hybridization and adjusting the electronic and magnetic structures of the Co/BP interface

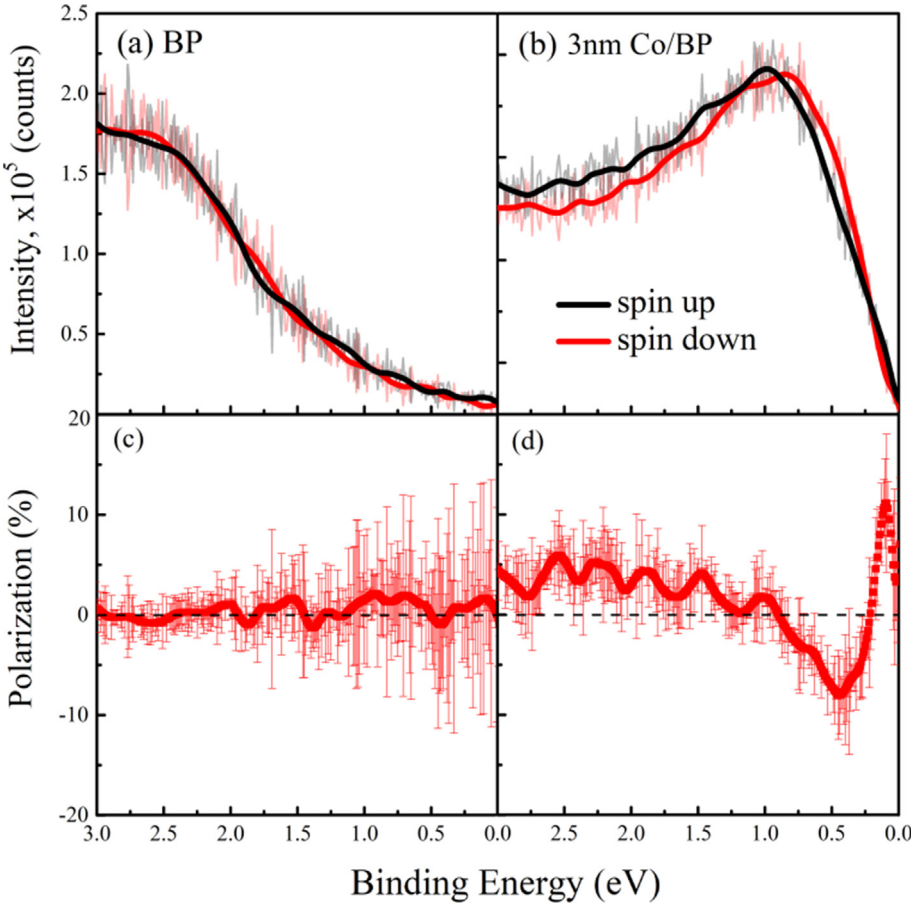

Fig. 5. Spin-polarized ultraviolet photoemission spectra of (a) BP and (b) 3nm Co/BP. Black lines: spin-up, red lines: spin down, original curve is shown in translucent color. The corresponding spin polarization (c), (d).

are helpful to reduce the spin loss of spintronic devices. In addition, by controlling the spin polarization inversion near E_F, different spin electrons can be selectively injected from the same ferromagnetic electrode.

4. Conclusions

In conclusion, we have investigated the electronic properties and spin polarization of the Co/BP interface using XPS, UPS, and SR-UPS. The results show that the unbonded P appears when the outermost BP lattice is destroyed by the deposition of Co and an interface dipole is observed at Co/BP interface. There is no chemical reaction between Co and BP or unbonded P. The inverted spin polarization near E_F has been observed and it can be attributed to the interface hybridization between Co and BP. It is indicated that Co/BP interface can be used to design Co/BP-based spintronic devices and interface modified is necessary.

CRediT authorship contribution statement

Baoxing Liu: Conceptualization, Investigation, Formal analysis, Writing - original draft. **Haipeng Xie:** Writing - review & editing, Project administration, Funding acquisition. **Yuquan Liu:** Formal analysis, Visualization. **Can Wang:** Formal analysis, Visualization. **Shitan Wang:** Investigation. **Yuan Zhao:** Investigation. **Jinxin Liu:** Investigation. **Dongmei Niu:** Methodology. **Han Huang:** Methodology. **Yongli Gao:** Writing - review & editing, Supervision, Funding acquisition.

Declaration of Competing Interest

The authors declare that they have no known competing financial interests or personal relationships that could have appeared to influence the work reported in this paper.

Acknowledgments

We thank the financial support by the National Key Research and Development Program of China (Grant Nos. 2017YFA0206602), the National Natural Science Foundation of China (Grant Nos. 11334014 and 51802355), and National Key Laboratory Open Project Foundation (Grant No. 165000001). H.X. acknowledges the support by the Natural Science Foundation of Hunan Province (Grant No. 2018JJ3625). Y. G. acknowledges the support from National Science Foundation (DMR-1903981 and 1903962).

Appendix A. Supplementary data

Supplementary data to this article can be found online at https://doi.org/10.1016/j.jmmm.2019.166297.

References

[1] A.K. Geim, K.S. Novoselov, The rise of graphene, Nat. Mater. 6 (3) (2007) 183–191.
[2] K.I. Bolotin, K.J. Sikes, Z. Jiang, M. Klima, G. Fudenberg, J. Hone, P. Kim, H.L. Stormer, Ultrahigh electron mobility in suspended graphene, Solid State Commun. 146 (9–10) (2008) 351–355.
[3] K.S. Novoselov, A.K. Geim, S.V. Morozov, D. Jiang, M.I. Katsnelson, I.V. Grigorieva, S.V. Dubonos, A.A. Firsov, Two-dimensional gas of massless Dirac fermions in graphene, Nature 438 (7065) (2005) 197–200.
[4] Y. Zhang, Y.W. Tan, H.L. Stormer, P. Kim, Experimental observation of the quantum Hall effect and Berry's phase in graphene, Nature 438 (7065) (2005) 201–204.
[5] A.H. Castro Neto, F. Guinea, N.M.R. Peres, K.S. Novoselov, A.K. Geim, The electronic properties of graphene, Rev. Mod. Phys. 81 (1) (2009) 109.

[6] F. Schwierz, Graphene transistors, Nat. Nanotechnol. 5 (7) (2010) 487–496.
[7] A. Avsar, J.Y. Tan, M. Kurpas, M. Gmitra, K. Watanabe, T. Taniguchi, J. Fabian, B. Ozyilmaz, Gate-tunable black phosphorus spin valve with nanosecond spin lifetimes, Nat. Phys. 13 (9) (2017) 888-+.
[8] M. Chhowalla, H.S. Shin, G. Eda, L.J. Li, K.P. Loh, H. Zhang, The chemistry of two-dimensional layered transition metal dichalcogenide nanosheets, Nat. Chem. 5 (4) (2013) 263–275.
[9] J.N. Coleman, M. Lotya, A. O'Neill, S.D. Bergin, P.J. King, U. Khan, K. Young, A. Gaucher, S. De, R.J. Smith, I.V. Shvets, S.K. Arora, G. Stanton, H.Y. Kim, K. Lee, G.T. Kim, G.S. Duesberg, T. Hallam, J.J. Boland, J.J. Wang, J.F. Donegan, J.C. Grunlan, G. Moriarty, A. Shmeliov, R.J. Nicholls, J.M. Perkins, E.M. Grieveson, K. Theuwissen, D.W. McComb, P.D. Nellist, V. Nicolosi, Two-dimensional nanosheets produced by liquid exfoliation of layered materials, Science 331 (6017) (2011) 568–571.
[10] M.V. Kamalakar, B.N. Madhushankar, A. Dankert, S.P. Dash, Low Schottky barrier black phosphorus field-effect devices with ferromagnetic tunnel contacts, Small 11 (18) (2015) 2209–2216.
[11] F.N. Xia, H. Wang, Y.C. Jia, Rediscovering black phosphorus as an anisotropic layered material for optoelectronics and electronics, Nat. Commun. 5 (2014) 4458.
[12] H. Liu, A.T. Neal, Z. Zhu, Z. Luo, X. Xu, D. Tomanek, P.D. Ye, Phosphorene: an unexplored 2D semiconductor with a high hole mobility, ACS Nano 8 (4) (2014) 4033–4041.
[13] L. Li, Y. Yu, G.J. Ye, Q. Ge, X. Ou, H. Wu, D. Feng, X.H. Chen, Y. Zhang, Black phosphorus field-effect transistors, Nat. Nanotechnol. 9 (5) (2014) 372–377.
[14] L. Li, M. Engel, D.B. Farmer, S.J. Han, H.S. Wong, High-performance p-type black phosphorus transistor with scandium contact, Acs Nano 10 (4) (2016) 4672–4677.
[15] J. Dai, X.C. Zeng, Bilayer phosphorene: effect of stacking order on bandgap and its potential applications in thin-film solar cells, J. Phys. Chem. Lett. 5 (7) (2014) 1289–1293.
[16] S.P. Dash, S. Sharma, R.S. Patel, M.P. de Jong, R. Jansen, Electrical creation of spin polarization in silicon at room temperature, Nature 462 (7272) (2009) 491–494.
[17] Y.L. Du, C.Y. Ouyang, S.Q. Shi, M.S. Lei, Ab initio studies on atomic and electronic structures of black phosphorus, J. Appl. Phys. 107 (9) (2010) 093718.
[18] O. Prytz, E. Flage-Larsen, The influence of exact exchange corrections in van der Waals layered narrow bandgap black phosphorus, J. Phys. Condens. Matter 22 (1) (2010) 015502.
[19] S. Narita, Y. Akahama, Y. Tsukiyama, K. Muro, S. Mori, S. Endo, M. Taniguchi, M. Seki, S. Suga, A. Mikuni, Electrical and optical properties of black phosphorus single crystals, Physica B+C 117 (1983) 422–424.
[20] Y. Maruyama, S. Suzuki, K. Kobayashi, S. Tanuma, Synthesis and some properties of black phosphorus single crystals, Physica B+C 105 (1) (1981) 99–102.
[21] A.S. Rodin, A. Carvalho, A.H. Castro Neto, Strain-induced gap modification in black phosphorus, Phys. Rev. Lett. 112 (17) (2014) 176801.
[22] Q.H. Liu, X.W. Zhang, L.B. Abdalla, A. Fazzio, A. Zunger, Switching a normal insulator into a topological insulator via electric field with application to phosphorene, Nano Lett. 15 (2) (2015) 1222–1228.
[23] M.Y. Chen, Z.Z. Yu, Y. Wang, Y.Q. Xie, J. Wang, H. Guo, Nonequilibrium spin injection in monolayer black phosphorus, Phys. Chem. Chem. Phys. 18 (3) (2016) 1601–1606.
[24] L.L. Xu, J.F. Feng, K.K. Zhao, W.M. Lv, X.F. Han, Z.Y. Liu, X.H. Xu, H. Huang, Z.M. Zeng, Magnetoresistance effect in NiFe/BP/NiFe vertical spin valve devices, Adv. Condensed Matter Phys. 2017 (2017).
[25] R. Lin, F. Wang, J. Rybicki, M. Wohlgenannt, K.A. Hutchinson, Distinguishing between tunneling and injection regimes of ferromagnet/organic semiconductor/ferromagnet junctions, Phys. Rev. B 81 (19) (2010) 195214.
[26] Z.H. Xiong, D. Wu, Z.V. Vardeny, J. Shi, Giant magnetoresistance in organic spin-valves, Nature 427 (6977) (2004) 821–824.
[27] X.L. Sui, C. Si, B. Shao, X.L. Zou, J. Wu, B.L. Gu, W.H. Duan, Tunable magnetism in transition-metal-decorated phosphorene, J. Phys. Chem. C 119 (18) (2015) 10059–10063.
[28] L. Schulz, L. Nuccio, M. Willis, P. Desai, P. Shakya, T. Kreouzis, V.K. Malik, C. Bernhard, F.L. Pratt, N.A. Morley, Engineering spin propagation across a hybrid organic/inorganic interface using a polar layer, Nat. Mater. 10 (1) (2011) 39.
[29] D.L. Sun, M. Fang, X.S. Xu, L. Jiang, H.W. Guo, Y.M. Wang, W.T. Yang, L.F. Yin, P.C. Snijders, T.Z. Ward, Z. Gai, X.G. Zhang, H.N. Lee, J. Shen, Active control of magnetoresistance of organic spin valves using ferroelectricity, Nat. Commun. 5 (2014) 4396.
[30] C. Barraud, P. Seneor, R. Mattana, S. Fusil, K. Bouzehouane, C. Deranlot, P. Graziosi, L. Hueso, I. Bergenti, V. Dediu, F. Petroff, A. Fert, Unravelling the role of the interface for spin injection into organic semiconductors, Nat. Phys. 6 (8) (2010) 615–620.
[31] N. Atodiresei, J. Brede, P. Lazic, V. Caciuc, G. Hoffmann, R. Wiesendanger, S. Blugel, Design of the local spin polarization at the organic-ferromagnetic interface, Phys. Rev. Lett. 105 (6) (2010) 066601.
[32] H.P. Xie, H. Huang, N.T. Cao, C.H. Zhou, D.M. Niu, Y.L. Gao, Effects of annealing on structure and composition of LSMO thin films, Phys. B-Condensed Matter 477 (2015) 14–19.
[33] Y. Zhao, X.L. Liu, L. Lyu, L. Li, W.J. Tan, S.T. Wang, C. Wang, D.M. Niu, H.P. Xie, H. Huang, Fullerene (C_{60}) interlayer modification on the electronic structure and the film growth of 2, 7-diocty [1] benzothieno-[3, 2-b] benzothiophene on SiO 2, Synthetic Met. 229 (2017) 1–6.
[34] H.P. Xie, D.M. Niu, L. Lyu, H. Zhang, Y.H. Zhang, P. Liu, P. Wang, D. Wu, Y.L. Gao, Evolution of the electronic structure of $C_{60}/La_{0.67}Sr_{0.33}MnO_3$ interface, Appl. Phys. Lett. 108 (1) (2016) 011603.
[35] X.L. Liu, C.G. Wang, C.C. Wang, I.F. Irfan, Y.L. Gao, Interfacial electronic structures of buffer-modified pentacene/C-60-based charge generation layer, Org. Electron. 17 (2015) 325–333.
[36] X.L. Liu, C.G. Wang, Irfan, S.J. Yi, Y.L. Gao, Effect of oxygen plasma treatment on air exposed MoO_x thin film, Org. Electron. 15 (5) (2014) 977–983.
[37] B.X. Liu, H.P. Xie, D.M. Niu, H. Huang, C. Wang, S.T. Wang, Y. Zhao, Y.Q. Liu, Y.L. Gao, Interface electronic structure between Au and black phosphorus, J. Phys. Chem. C 122 (32) (2018) 18405–18411.
[38] N. Koch, A. Gerlach, S. Duhm, H. Glowatzki, G. Heimel, A. Vollmer, Y. Sakamoto, T. Suzuki, J. Zegenhagen, J.P. Rabe, F. Schreiber, Adsorption-induced intramolecular dipole: correlating molecular conformation and interface electronic structure, J. Am. Chem. Soc. 130 (23) (2008) 7300–7304.
[39] M. Fahlman, A. Crispin, X. Crispin, S.K. Henze, M.P. de Jong, W. Osikowicz, C. Tengstedt, W.R. Salaneck, Electronic structure of hybrid interfaces for polymer-based electronics, J. Phys. Condens. Matter 19 (18) (2007) 183202.
[40] H. Yoshida, A. Terasaki, K. Kobayashi, M. Tsukada, T. Kondow, Spin-polarized electronic structure of cobalt cluster anions studied by photoelectron spectroscopy, J. Chem. Phys. 102 (15) (1995) 5960–5965.
[41] L. Lozzi, S. Santucci, S. La Rosa, Au/CuPc interface: photoemission investigation, J. Vacuum Sci. Technol. A 22 (4) (2004) 1477–1481.
[42] C.E. Myers, H.F. Franzen, J.W. Anderegg, X-ray photoelectron spectra and bonding in transition-metal phosphides, Inorg. Chem. 24 (12) (1985) 1822–1824.
[43] R. Zan, Q.M. Ramasse, R. Jalil, T. Georgiou, U. Bangert, K.S. Novoselov, Control of radiation damage in MoS_2 by graphene encapsulation, ACS Nano 7 (11) (2013) 10167–10174.
[44] Y. Liu, J. Guo, E. Zhu, L. Liao, S.J. Lee, M. Ding, I. Shakir, V. Gambin, Y. Huang, X. Duan, Approaching the Schottky-Mott limit in van der Waals metal-semiconductor junctions, Nature 557 (7707) (2018) 696–700.
[45] W.E. Spicer, P.W. Chye, C.M. Garner, I. Lindau, P. Pianetta, The surface electronic structure of 3–5 compounds and the mechanism of Fermi level pinning by oxygen (passivation) and metals (Schottky barriers), Surf. Sci. 86 (1979) 763–788.
[46] W.R. Salaneck, K. Seki, A. Kahn, J.-J. Pireaux, Conjugated Polymer and Molecular Interfaces: Science and Technology for Photonic and Optoelectronic Application, CRC Press, New York, 2001.
[47] Y.L. Gao, Surface analytical studies of interfaces in organic semiconductor devices, Mat. Sci. Eng. R. 68 (3) (2010) 39–87.
[48] X.L. Liu, C.G. Wang, L. Lyu, C.C. Wang, Z.G. Xiao, C. Bi, J.S. Huang, Y.L. Gao, Electronic structures at the interface between Au and $CH_3NH_3PbI_3$, Phys. Chem. Chem. Phys. 17 (2) (2015) 896–902.
[49] M.P. Seah, W. Dench, Quantitative electron spectroscopy of surfaces: a standard data base for electron inelastic mean free paths in solids, Surface Interface Anal. 1 (1) (1979) 2–11.
[50] Y. Xiang, Q.L. Xia, J.H. Luo, Y.P. Liu, Y.D. Peng, D.W. Wang, Y.Z. Nie, G.H. Guo, Observation of ferromagnetism in black phosphorus nanosheets with high magnetization by liquid exfoliation, Solid State Commun. 281 (2018) 1–5.
[51] J. Wang, D. Liu, H. Huang, N. Yang, B. Yu, M. Wen, X. Wang, P.K. Chu, X.F. Yu, In-plane black phosphorus/dicobalt phosphide heterostructure for efficient electrocatalysis, Angew Chem Int Ed Engl 57 (10) (2018) 2600–2604.
[52] J.F. Callejas, C.G. Read, E.J. Popczun, J.M. McEnaney, R.E. Schaak, Nanostructured Co_2P electrocatalyst for the hydrogen evolution reaction and direct comparison with morphologically equivalent CoP, Chem. Mater. 27 (10) (2015) 3769–3774.
[53] F. Djeghloul, M. Gruber, E. Urbain, D. Xenioti, L. Joly, S. Boukari, J. Arabski, H. Bulou, F. Scheurer, F. Bertran, P. Le Fevre, A. Taleb-Ibrahimi, W. Wulfhekel, G. Garreau, S. Hajjar-Garreau, P. Wetzel, M. Alouani, E. Beaurepaire, M. Bowen, W. Weber, High spin polarization at ferromagnetic metal-organic interfaces: a generic property, J. Phys. Chem. Lett. 7 (13) (2016) 2310–2315.
[54] V. Dediu, L.E. Hueso, I. Bergenti, A. Riminucci, F. Borgatti, P. Graziosi, C. Newby, F. Casoli, M.P. De Jong, C. Taliani, Room-temperature spintronic effects in Alq_3-based hybrid devices, Phys. Rev. B 78 (11) (2008) 115203.
[55] D. Sun, L. Yin, C. Sun, H. Guo, Z. Gai, X.G. Zhang, T.Z. Ward, Z. Cheng, J. Shen, Giant magnetoresistance in organic spin valves, Phys. Rev. Lett. 104 (23) (2010) 236602.
[56] S. Wang, Y.J. Shi, L. Lin, B.B. Chen, F.J. Yue, J. Du, H.F. Ding, F.M. Zhang, D. Wu, Room-temperature spin valve effects in $La_{0.67}Sr_{0.33}MnO_3/Alq_3/Co$ devices, Synthetic Met. 161 (15–16) (2011) 1738–1741.